TEPHRA SAMPLES AND ANALYSES FROM THE 2018–2023 ERUPTION OF SEMISOPOCHNOI VOLCANO, ALASKA

Matthew W. Loewen, Hannah R. Dietterich, Jordan Lubbers, and Alexa R. Van Eaton

Raw Data File 2025-15

2025
STATE OF ALASKA
DEPARTMENT OF NATURAL RESOURCES
DIVISION OF GEOLOGICAL & GEOPHYSICAL SURVEYS

STATE OF ALASKA
Mike Dunleavy, Governor

DEPARTMENT OF NATURAL RESOURCES
John Boyle, Commissioner

DIVISION OF GEOLOGICAL & GEOPHYSICAL SURVEYS
Jennifer Athey, Acting State Geologist & Director

Publications produced by the Division of Geological & Geophysical Surveys are available to download from the DGGS website (dggs.alaska.gov). Publications on hard-copy or digital media can be examined or purchased in the Fairbanks office:

Alaska Division of Geological & Geophysical Surveys (DGGS)
3354 College Road | Fairbanks, Alaska 99709-3707
Phone: 907.451.5010 | Fax 907.451.5050
dggspubs@alaska.gov | dggs.alaska.gov

DGGS publications are also available at:

Alaska State Library, Historical
Collections & Talking Book Center
395 Whittier Street
Juneau, Alaska 99801

Alaska Resource Library and
Information Services (ARLIS)
3150 C Street, Suite 100
Anchorage, Alaska 99503

Suggested citation:
Loewen, M.W., Dietterich, H.R., Lubbers, Jordan, and Van Eaton, A.R., 2025, Tephra samples and analyses from the 2018-2023 eruption of Semisopochnoi Volcano, Alaska: Alaska Division of Geological & Geophysical Surveys Raw Data File 2025-15, 13 p. https://doi.org/10.14509/31645

TEPHRA SAMPLES AND ANALYSES FROM THE 2018–2023 ERUPTION OF SEMISOPOCHNOI VOLCANO, ALASKA

Matthew W. Loewen[1], Hannah R. Dietterich[1], Jordan Lubbers[1], and Alexa R. Van Eaton[2]

INTRODUCTION

This report includes samples and analyses collected from the 2018–2023 eruption of Semisopochnoi volcano in the western Aleutian Islands, Alaska. Samples were collected during two field visits: May 30 to June 1, 2021, and June 10, 2023. A total of sixteen samples were collected across Semisopochnoi Island at varying distances from the eruption source, the north crater of Mount Young (fig. 1). Samples were collected from the surface on snow, grass, or other substrates that suggested deposition during recent eruptive activity but are, in all cases, aggregates of prior eruption events up to the sample date and may contain minor wind-blown contamination from older surfaces.

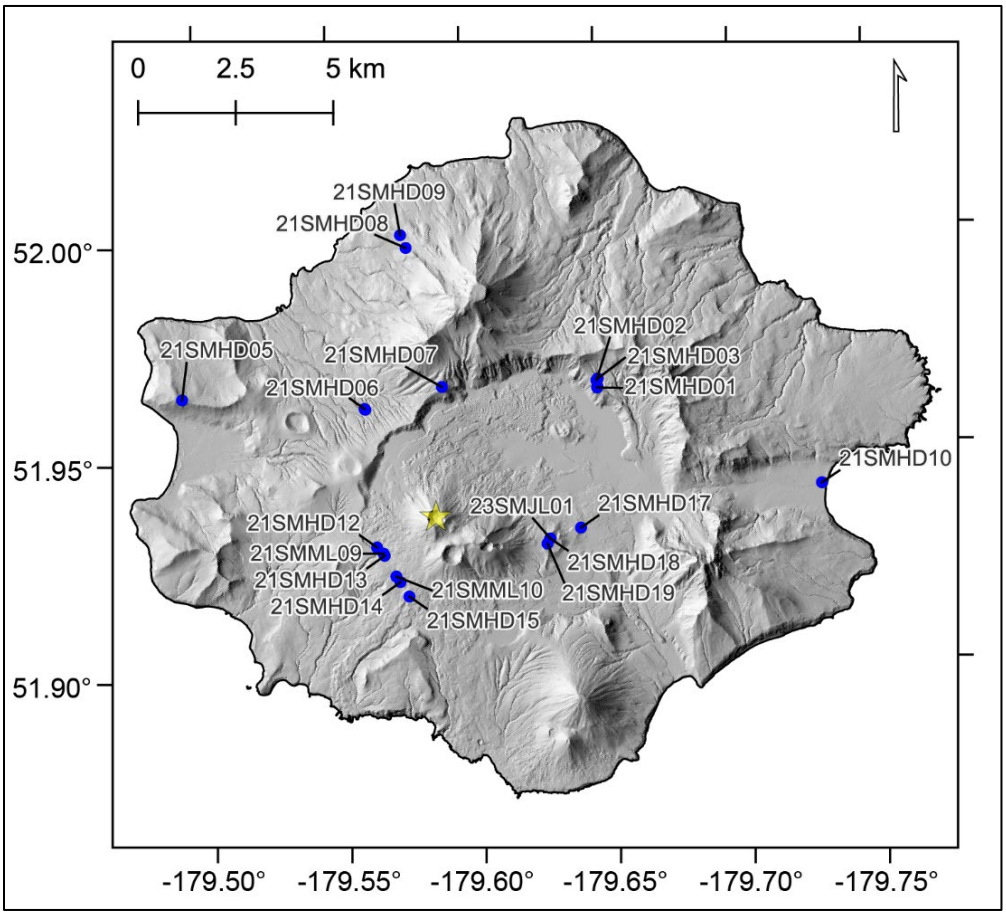

Figure 1. Hillshade map of Semisopochnoi Island and the locations of sample and observation stations (blue circles) in this report. The north crater of Mount Young, the source vent for the 2018–2023 eruption, is marked with a yellow star. Hillshade derived from IFSAR.

[1] U.S. Geological Survey, Alaska Volcano Observatory, 4230 University Dr., Anchorage, Alaska 99508

[2] U.S. Geological Survey, Cascade Volcano Observatory, 1300 SE Cardinal Court, Vancouver, Washington 98683

Data associated with this report are available at doi.org/10.14509/31645, and a subset of the results are archived in the Geologic Database of Information on Volcanoes in Alaska (GeoDIVA; Cameron and others, 2022, doi.org/10.14509/geodiva). Tables include:

- **Definitions**: Descriptions (i.e., units, methods) for all columns in other data tables.
- **Stations**: Site (station) coordinates, description, and observations.
- **Samples**: Metadata for collected samples. Samples can be linked to the Stations data through the StationID column.
- **GrainSize**: Grain size distribution results from multiple methods. This table can be linked to the Samples table by the SampleID and at_num columns.
- **EPMA**: Electron probe microanalysis matrix glass analyses. This table can be linked to the Samples table by the SampleID and at_num columns.
- **Componentry**: Componentry classification from the 250–500 µm size fraction. This table can be linked to the Samples table by the SampleID and at_num columns.
- **MeasuredArea**: Mass per unit area results for three measured area field samples. This table can be linked to the Samples table by the SampleID and at_num columns.

METHODS

Field Data

Samples were collected in 2021 and 2023. Locations were determined using built-in GPS on tablet devices and are accurate to ~10 m. Coordinates were recorded in WGS84 datum. Station names (StationID) were assigned to sample locations and sites of general observation (fig. 1); sample names (SampleID) correspond to specific samples and include sample descriptions. Laboratory id numbers (at_num) were assigned during laboratory processing and analysis.

Grain size analysis

Grain size distributions for nine bulk samples were determined by three different methods: standard sieving, laser diffraction particle size analysis, and dynamic image analysis.

Sieving was performed in the U.S. Geological Survey Alaska Tephra Laboratory in Anchorage, Alaska. A 20–30 g split of material was disaggregated in a sonic bath before wet sieving through 500 µm, 250 µm, 125 µm, and 63 µm disposable meshes. The less than 63 µm fraction was allowed to settle in a beaker, decanted, and poured through Whatman 541 filter paper. Loss of particles less than 22 µm through the filter paper can be up to 0.3 percent, which is negligible relative to the overall grain size distribution. Material from each sieve fraction was dried for more than 24 hours at 40–50 ˚C and weighed on calibrated scales. The more than 500 µm size fraction was further dry sieved with 1 mm, 2 mm, or 4 mm metal sieves. Data are reported as a percentage of total mass for each 1-phi grain-size bin.

A split of each bulk, unprocessed sample was analyzed with a Beckman Coulter LS 13 320 laser diffraction (LD) particle size analyzer at the U.S. Geological Survey Cascades Volcano Observatory in Vancouver, Washington. This instrument analyzes particles less than 1 mm in a

water suspension that circulates past a laser, using Mie scattering theory (Stratton, 2015) to convert the light scattering pattern into a particle size distribution. To prepare the material, a small aliquot of bulk sample was scooped out of the well-mixed bag and transferred to a watch glass. Material on the watch glass was manually disaggregated, taking care to break apart any cemented chunks without disrupting intact clasts. Fibrous organic material more than 0.25 mm was removed with forceps. Using deionized water, the entire prepared sample was passed through a 1 mm sieve directly into a circulating water bath known as the aqueous liquid module. To further break up aggregates, the mixture was then sonicated with an ultrasonic wand for at least 90 seconds before each analysis, and during three sequential, 60-second analyses. It is worth noting that a separate method of sample preparation was trialed and found to be unsuitable for these samples—pipetting an aliquot of water-suspended material artificially biased the sample because the coarse, denser grains settled too quickly. For analysis, the optical model assumed a refractive index of 1.54 and absorption coefficient of 0.001, which is a reasonable estimate for basaltic andesite (Vogel and others, 2017). Averaged results for each sample were binned into 0.5 phi intervals. Since the laser diffraction system only analyzes particles less than 1 mm, and most of the Semisopochnoi Island samples contained coarser material, the complete size distribution was calculated by merging LD data with the sieve data. Each LD size bin was multiplied by the fraction less than 1 mm determined from sieving, using standard methods (Mastin and others, 2020). These final, merged results are reported in the enclosed data tables.

Another 1–10 g aliquot of well-mixed bulk sample was separated for analysis with a Camsizer X2 dynamic image analyzer (DIA) at the U.S. Geological Survey Hawaii Volcano Observatory in Hilo, Hawaii. This instrument analyzes ash grains dispersed in compressed air with a high-speed camera and thus directly measures cross-sectional area of individual grains. Prior to analysis the sample was dried and large aggregates gently massaged apart by hand. Large organic material was removed with forceps.

Because all material in this sample suite was less than the maximum 4 mm-particle-size this instrument can analyze, no pre-sieving of the bulk sample was needed. Particles were analyzed with a 20 kPa dispersion pressure. While each sample analysis consisted of silhouette images of thousands of individual grains, data reported here are the summary statistics of the individual particle minimum maximum chord length (xc min) aggregated into 0.5 phi bins (Schmith and Swanson, 2023) resulting in a cross-sectional area-proportional grain size distribution.

All grain size distributions and methodologies are compared in figures 2 and 3. Table 1 includes overall grain size statistics from Folk and Ward (1957) calculated following the procedures outlined in Blott and Pye (2001). The “pan” fraction (less than 63 μm) by sieving includes 30–50 percent of the total mass, thus statistics are only appropriately applied to the DIA and merged LD sieve results.

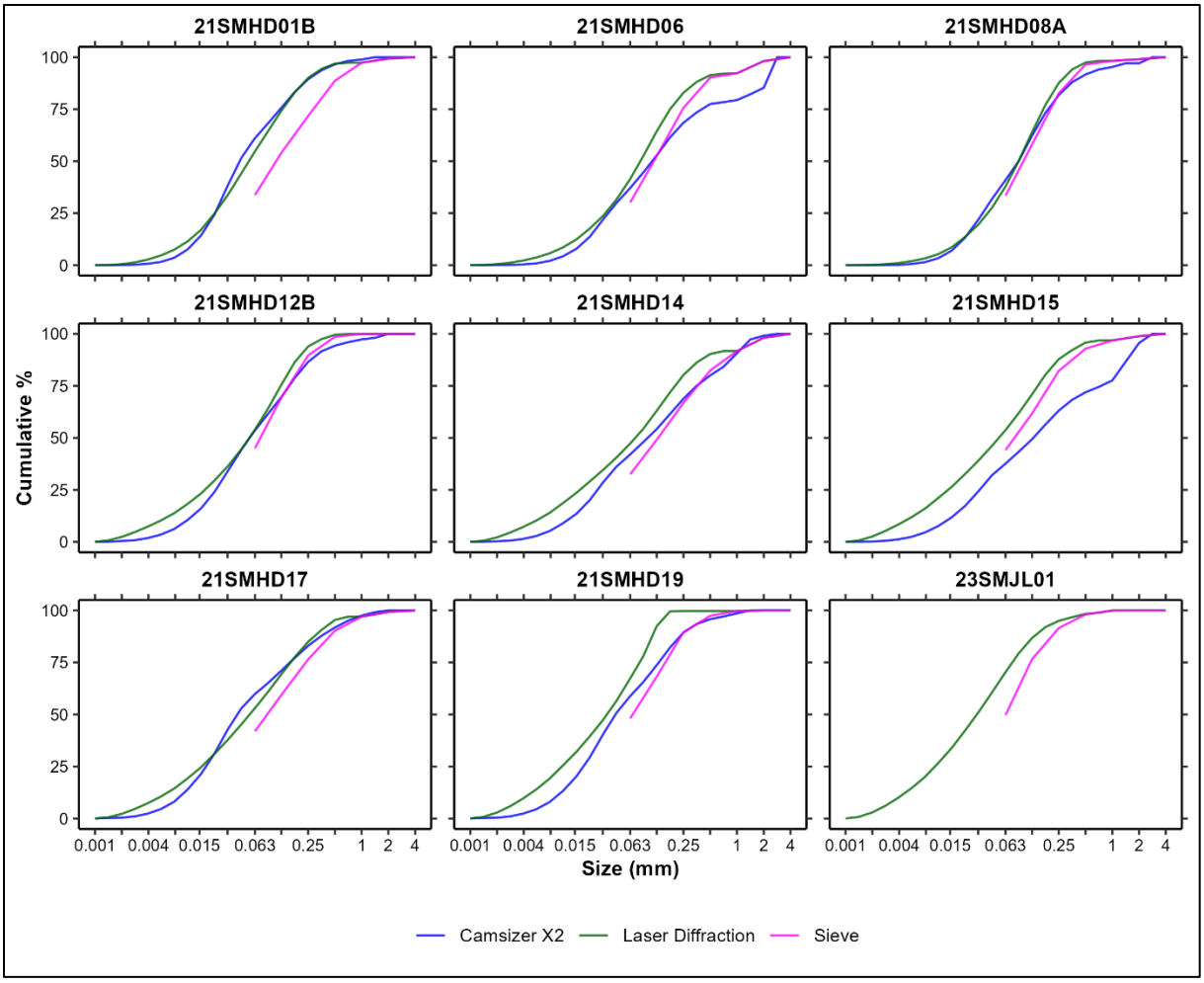

Figure 2. Cumulative grain size distributions for all Semisopochnoi ash samples and grain size analysis methods, compared on a sample-by-sample basis.

The LD and DIA instruments used here are typically restricted to less than 1 mm and less than 4 mm maximum grain sizes, respectively. Results are then typically merged with other methodologies for coarser size fractions (such as sieving or larger size DIA instruments such as the Camsizer P4; Schmith and Swanson, 2023). However, for these samples, all three methods can measure the majority of the grain size distribution, and methods can be directly compared, although we do merge the greater than 1 mm sieve results with the LD for best accuracy. From this comparison, we have made a few important notes on these three methods:

- We do not have data to evaluate accuracy of sieve data and acknowledge the limitation of only using whole-phi size bins. We note that with sonicator disaggregation followed immediately by wet sieving, only one sample (21SMHD06) had a second very coarse ash mode (table 1). Examination of this fraction, and minor very coarse fractions in other samples, suggests these are entirely lithic (non-juvenile) grains and represent wind-blown contamination of the original sample, not primary volcanic products from the eruption from the north crater of Semisopochnoi Island's Mount Young.

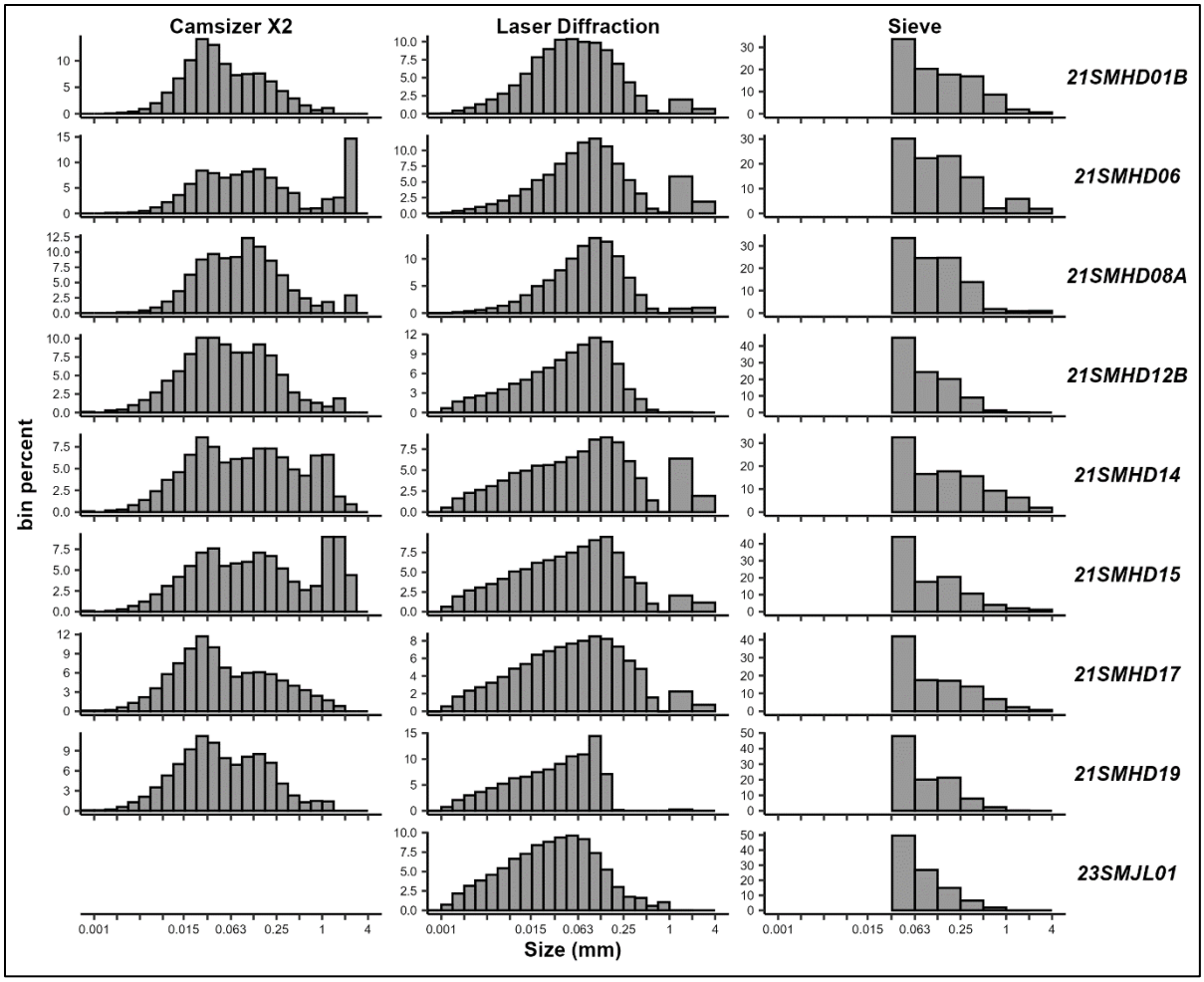

Figure 3. Individual sample histograms of ash grain size distribution from Semisopochnoi samples in this report. The rightmost bin of sieve material is the "pan" fraction and represents all less than 63 µm material but is plotted as the same width as other bins (1 phi). Note the changing bin-width of laser diffraction data, which reflects merging of 1 phi bin sieve data for material more than 1 mm, and thus the bin heights appear higher than they would if divided into the same 0.5 phi bin width of the other laser diffraction data.

- A prominent coarse mode is seen in many DIA analyses that is not seen, or is much less prominent, in sieve data (table 1; figs. 3 and 4). The coarse mode could be the result of particle aggregation—fine-grained Semisopochnoi ash readily cemented together in the lab. Effort was made to physically separate grains before DIA, and airflow within the Camsizer X2 also should help disaggregate grains; however, this may have been insufficient. Wet sieving and LD both involve suspension of grains in water that facilitates disaggregation. If this is the case, DIA may underestimate the proportion of fine-grained ash.

Table 1. Grainsize statistics for Semisopochnoi ash samples.

SampleID	MethodID	Pan (%)	Mean (µm)	Median (µm)	Modality	Mode 1 (µm)	Mode 2 (µm)	Mode 3 (µm)	Sorting	Skewness	Skew	Kurtosis
21SMHD01B	camsizer_x2	0	51	42	bimodal	26	148	*NA*	Poorly Sorted	Coarse Skewed	-0.20	0.94
21SMHD06	camsizer_x2	0	167	111	trimodal	2366	148	26	Very Poorly Sorted	Coarse Skewed	-0.29	1.06
21SMHD08A	camsizer_x2	0	85	88	trimodal	105	37	2366	Poorly Sorted	Symmetrical	-0.02	1.03
21SMHD12B	camsizer_x2	0	58	55	trimodal	26	37	148	Poorly Sorted	Symmetrical	-0.05	0.96
21SMHD14	camsizer_x2	0	107	99	trimodal	26	148	209	Very Poorly Sorted	Symmetrical	-0.03	0.81
21SMHD15	camsizer_x2	0	150	130	trimodal	1183	1673	37	Very Poorly Sorted	Symmetrical	-0.05	0.71
21SMHD17	camsizer_x2	0	51	40	bimodal	26	148	*NA*	Very Poorly Sorted	Coarse Skewed	-0.21	0.90
21SMHD19	camsizer_x2	0	47	43	bimodal	26	148	*NA*	Poorly Sorted	Symmetrical	-0.09	0.91
21SMHD01B	laser_diffrac	0	53	54	bimodal	52	1183	*NA*	Poorly Sorted	Symmetrical	0.05	0.98
21SMHD06	laser_diffrac	0	76	82	bimodal	105	1183	*NA*	Very Poorly Sorted	Symmetrical	0.01	1.30
21SMHD08A	laser_diffrac	0	79	88	unimodal	105	*NA*	*NA*	Poorly Sorted	Fine Skewed	0.17	1.03
21SMHD12B	laser_diffrac	0	44	55	unimodal	105	*NA*	*NA*	Very Poorly Sorted	Fine Skewed	0.26	0.95
21SMHD14	laser_diffrac	0	59	72	bimodal	148	1183	*NA*	Very Poorly Sorted	Symmetrical	0.10	1.03
21SMHD15	laser_diffrac	0	44	53	bimodal	148	1183	*NA*	Very Poorly Sorted	Fine Skewed	0.16	0.91
21SMHD17	laser_diffrac	0	49	55	bimodal	105	1183	*NA*	Very Poorly Sorted	Fine Skewed	0.13	0.91
21SMHD19	laser_diffrac	0	28	34	unimodal	105	*NA*	*NA*	Poorly Sorted	Fine Skewed	0.26	0.82
23SMJL01	laser_diffrac	0	27	30	unimodal	52	*NA*	*NA*	Very Poorly Sorted	Symmetrical	0.09	0.94
21SMHD01B	sieve	34	*NA*	*NA*	*NA*	75	*NA*	*NA*	*NA*	*NA*	*NA*	*NA*
21SMHD06	sieve	30	*NA*	*NA*	*NA*	148	1183	*NA*	*NA*	*NA*	*NA*	*NA*
21SMHD08A	sieve	33	*NA*	*NA*	*NA*	148	*NA*	*NA*	*NA*	*NA*	*NA*	*NA*
21SMHD12B	sieve	45	*NA*	*NA*	*NA*	75	*NA*	*NA*	*NA*	*NA*	*NA*	*NA*
21SMHD14	sieve	33	*NA*	*NA*	*NA*	148	*NA*	*NA*	*NA*	*NA*	*NA*	*NA*
21SMHD15	sieve	44	*NA*	*NA*	*NA*	148	*NA*	*NA*	*NA*	*NA*	*NA*	*NA*
21SMHD17	sieve	42	*NA*	*NA*	*NA*	75	*NA*	*NA*	*NA*	*NA*	*NA*	*NA*
21SMHD19	sieve	48	*NA*	*NA*	*NA*	148	*NA*	*NA*	*NA*	*NA*	*NA*	*NA*
23SMJL01	sieve	50	*NA*	*NA*	*NA*	75	*NA*	*NA*	*NA*	*NA*	*NA*	*NA*

Statistics follow methods outlined Folk and Ward (1957) and implimented in with R code that follows methods outlined in the GRADISTAT program by Blott and Pye (2001).

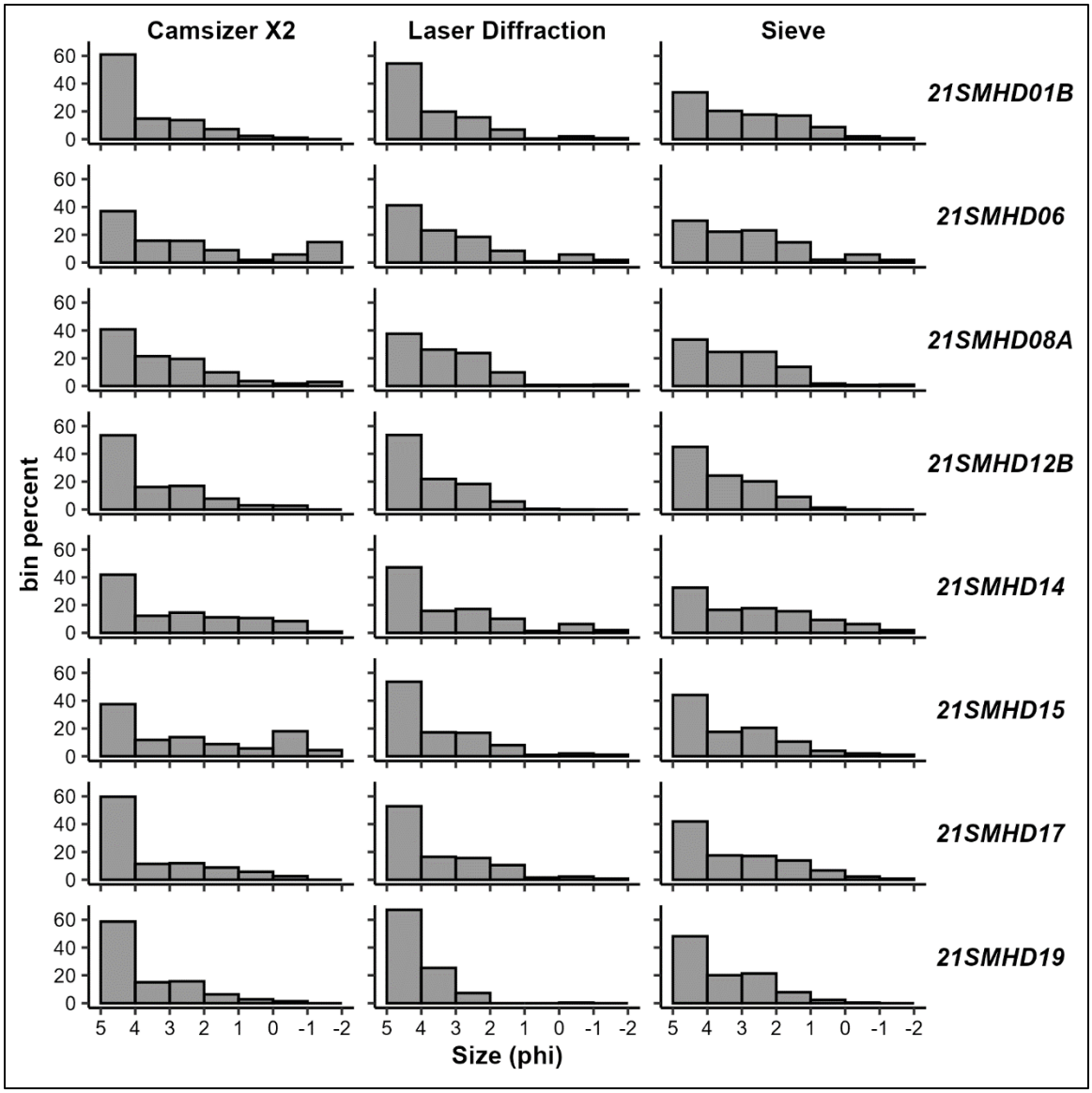

Figure 4. Individual sample histograms of ash grain size distribution from Semisopochnoi samples in this report combined into 1 phi bins with less than 63 µm (+4 phi) material combined into a common "pan" fraction.

- LD analyses result in higher estimates of 15 µm ash than DIA but tend to result in lower proportions of medium to coarse ash (less than 0.25 mm) than DIA or sieving. In an initial experiment, we used a pipette to subsample material for LD, and this resulted in an even larger underestimate of the medium and coarse ash. While this underrepresentation of medium to coarse ash was improved by not using the pipette subsampling method, we still see this fraction underrepresented compared to sieve results. This underrepresentation of medium and coarse ash may be an artifact of the LD assumptions (particle refractive index, assumption of spherical grains) and (or) proprietary curve-fitting algorithms of the instrument's software (Beckman Coulter, 2019). It is more difficult to determine if the less

than15 μm sizes are better analyzed by LD or DIA—as discussed above, cemented aggregates that were difficult to disaggregate may have reduced the finest particles measurable by DIA. Alternatively, assumptions in LD may overestimate their abundance. Further methodological comparisons are warranted but beyond the scope of this raw data report.

The application of three grain size methods to these samples, and unique properties of the Semisopochnoi volcano eruption, highlight several areas for methods development in grain size analysis of volcanic deposits. Very fine-grained, cemented ash was difficult to fully disaggregate in the lab without dedicated and time-consuming effort. The samples also included variable and sometimes significant amounts of fine, fibrous organic matter contamination. While larger pieces could be manually removed, very small organic fragments require more complicated processing which we did not undertake. This results in an unknown factor that could result in variability of our results. Thus, sample handling, preparation and subsampling before and during analysis can introduce significant variations in the results from sieving, LD, and DIA. In the future, we recommend synchronizing sample preparation methods across sieving, laser diffraction, and dynamic image analysis to improve the data comparability. Despite these difficulties, an important conclusion from this data set is that all three methods generate the same primary observation: samples from the 2018–2021 eruption of Semisopochnoi volcano contain abundant fine ash for the deposition distance from the source vent.

Electron Microprobe Analyses

Tephra samples were mounted in epoxy and polished for electron probe microanalysis (EPMA) in the Alaska Tephra Laboratory. Analyses were performed at the University of Alaska Fairbanks Advanced Instrumentation Lab on a JEOL JXA 8530F instrument in Fairbanks, Alaska. Detailed methodology and analysis of accuracy and precision can be found in Loewen and others (2023).

Results were manually filtered for low or high analytical totals or obvious beam interaction with mineral phases. Only 2 of 38 analyses were rejected. Results are shown here as Harker diagrams (fig. 5). Glass composition is mostly clustered between 63.4 and 66.3 weight percent SiO_2 with two outlier grains at 57.0 and 57.7 weight percent SiO_2.

Componentry Determination

Polished epoxy mounts were prepared for three size fractions (63–125 μm, 125–250 μm, and 250–500 μm) per sample. All three size fractions were qualitatively examined at the Alaska Tephra Laboratory on a JEOL 6510LV scanning electron microscope. There is apparent difference in component types or abundances between size fractions. Proportions of different components were ultimately quantified on backscatter electron image mosaics from the 250–500 μm size fraction into the following categories (fig. 6):

- **Glassy**: Characterized by clean interstitial glass in a microlitic matrix. Grains are typically dense, but occasionally vesicular grains are present. All EPMA analyses are from this component and on this 250–500 μm size fraction.

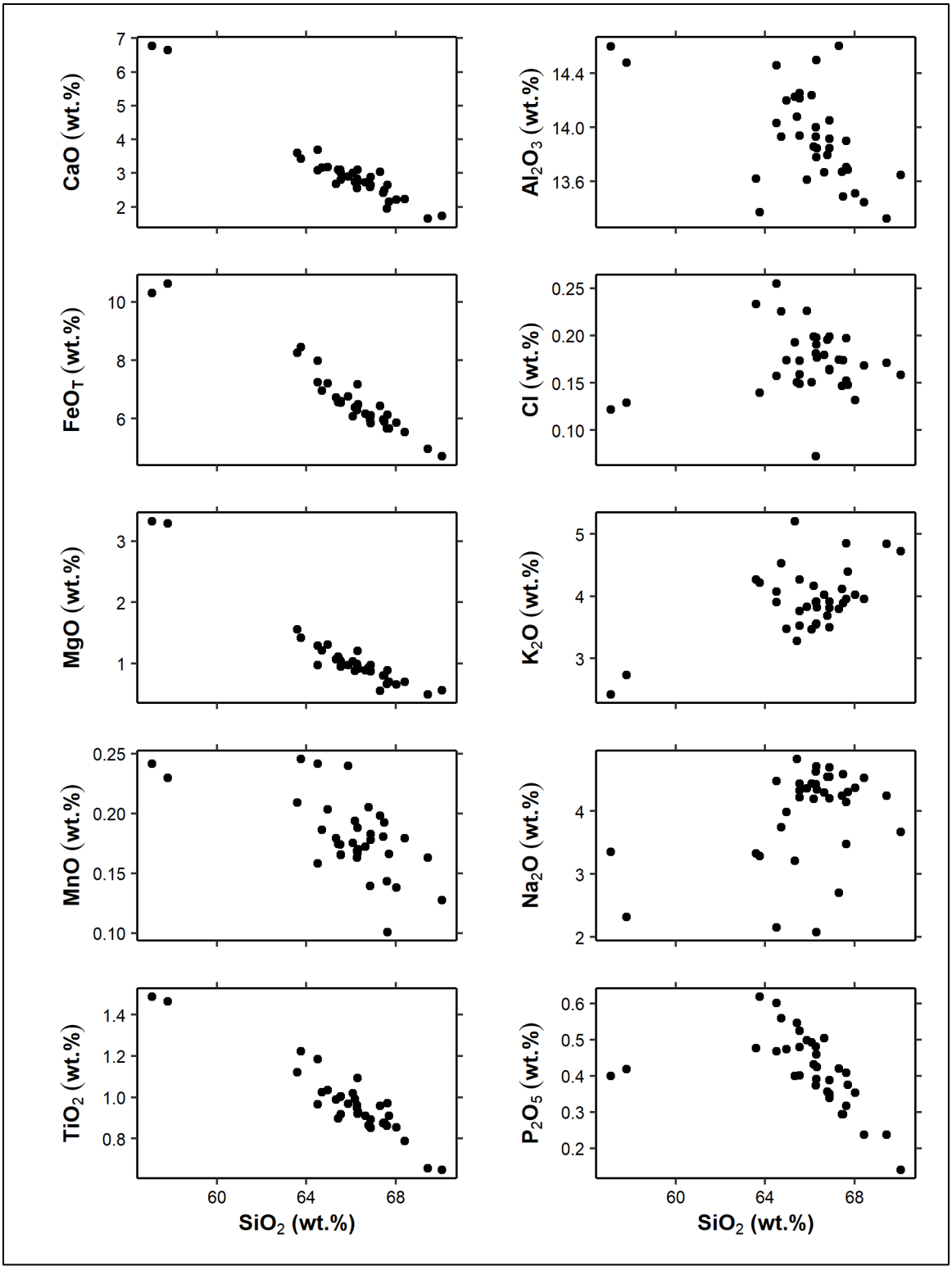

Figure 5. Harker diagrams of electron probe microanalysis glass analyses (EPMA) from three Semisopochnoi samples collected in 2021. Results were normalized to 100 percent anhydrous before plotting.

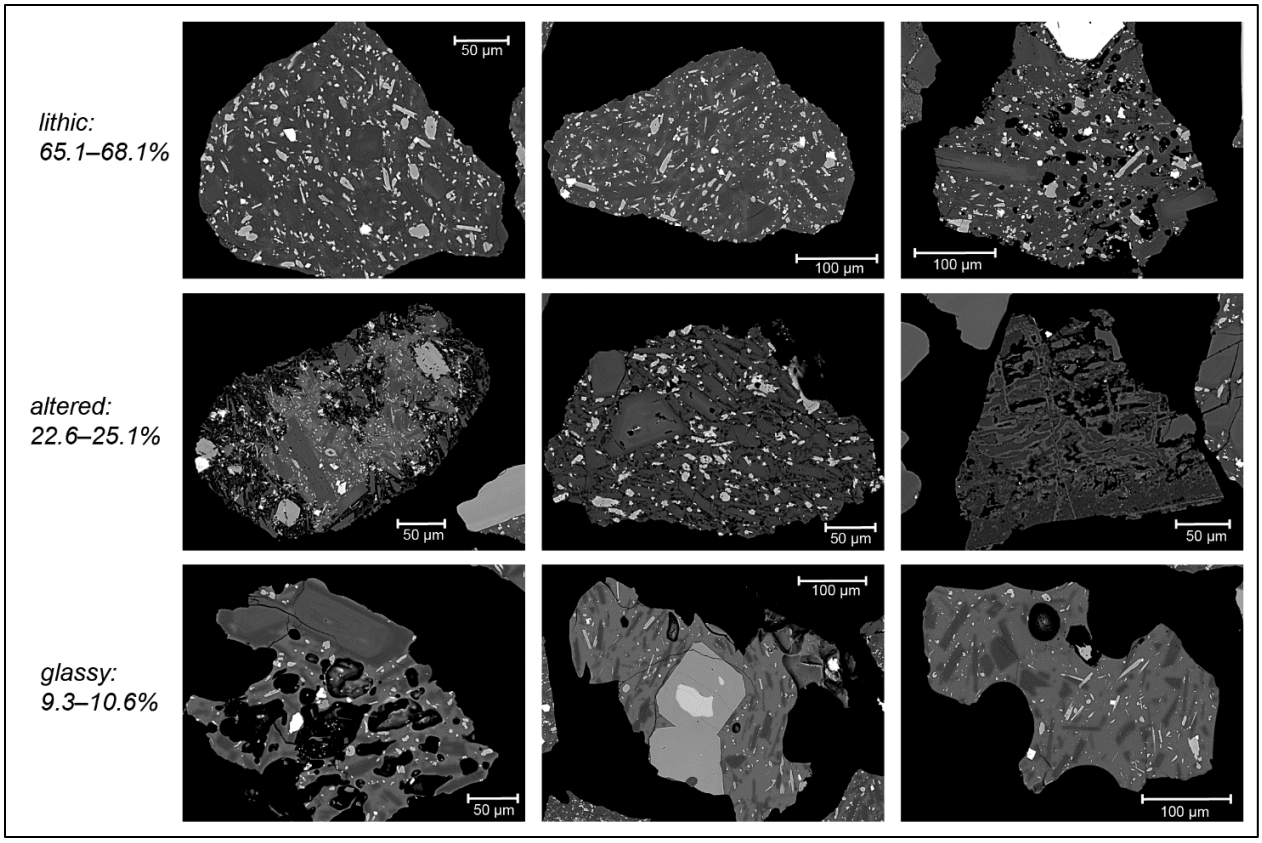

Figure 6. Representative component types and proportions in Semisopochnoi ash grains collected in 2021.

- **Lithic**: Characterized by the absence or near absence of glass and have dense microlitic groundmass. A very small remnant of interstitial glass may be present but occupies less than 5 µm areas and could not be easily analyzed by EPMA. Microlites are similar to those found in the glassy component although Fe-Ti oxides are more apparent (likely resulting from late-stage groundmass crystallization). Grains are typically dense with rare irregular vesicles.
- **Altered**: Characterized by grains with obvious alteration features. These features include (1) grains with interlocking crystals, angular void spaces, and no glass; (2) grains cored with regions of microlitic glass but eroded edges where glass is missing; and (3) grains with partial or total replacement of primary groundmass with feathery-textured alteration minerals such as clays.
- **Crystal**: Characterized by large loose phenocrysts of plagioclase, orthopyroxene, clinopyroxene, and Fe-Ti oxides. Inclusions of olivine were seen within other minerals (e.g., orthopyroxene). When adhering matrix is large enough to confidently identify, these are classified by prior components; otherwise, they are included simply as a crystal component.

Backscatter electron mosaics with marked classification components are provided as supplemental files with this report. The different classifications naturally grade into each other: glassy grains are somewhat gradational into lithic grains, and lithic and glassy grains can have less

obvious alteration features when examined in detail. As a result, the choice of these classifications is somewhat subjective. Examples of these components in unpolished grains are shown in figure 7.

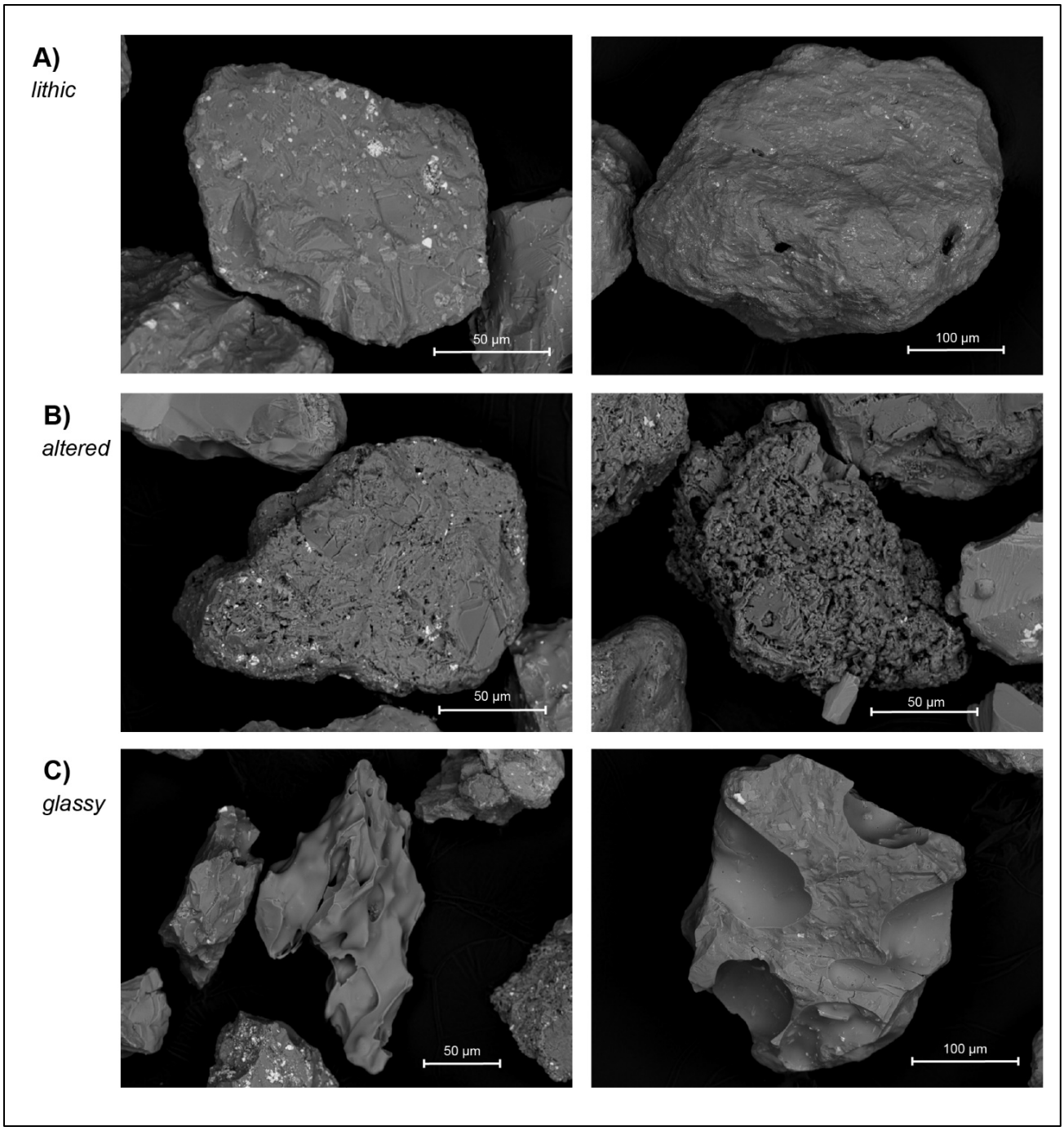

Figure 7. Example component types of unpolished grains using backscatter electron imaging.

Measured Area

At three field locations visited in early summer 2021, we collected ash that was deposited as a clear layer on top of clean snow from winter 2020 to spring 2021. Two of the sites (21SMHD19 and 21SMHD07) were collected in a 30 x 30 cm square, and one site (21SMHD12B) was collected over a 20 x 20 cm square. Ash and snow were collected in gallon sealable plastic bags, gravity filtered through Whatman 541 filter paper, and dried at 40–50 ˚C for more than 24 hours before weighing.

ACKNOWLEDGMENTS

Field sampling in 2021 and 2023 was conducted in association with Alaska Volcano Observatory geophysical monitoring network maintenance, with logistical support from field engineers on the joint mission. The 2021 work was supported by the crew of the R/V Steadfast and helicopter pilot Mike Grover. The 2023 work was supported by the crew of the R/V Tiĝlax̂. Simone Montayne provided metadata review. Kristi Wallace, Cheryl Cameron, and Scott Crass provided data and subject matter metadata review. Any use of trade, firm, or product names is for descriptive purposes only and does not imply endorsement by the U.S. Government.

REFERENCES

Beckman Coulter, 2019, User manual: LS 13 320 Laser diffraction particle size analyzer : Document number B05577.AD, 266 p. Accessible online: https://www.beckman.com/search#q=LS%2013%20320&t=coveo-tab-techdocs.

Blott, S.J., and Pye, Kenneth, 2001, GRADISTAT: A grain size distribution and statistics package for the analysis of unconsolidated sediments: Earth Surface Processes and Landforms, v. 26, no. 11, p. 1,237–1,248. https://doi.org/10.1002/esp.261

Cameron, C.E., Crass, S.W., and AVO Staff, eds., 2022, Geologic Database of Information on Volcanoes in Alaska (GeoDIVA): Alaska Division of Geological & Geophysical Surveys Digital Data Series 20, https://doi.org/10.14509/geodiva. https://doi.org/10.14509/30901

Folk, R.L., and Ward, W.C., 1957, Brazos River bar [Texas]; a study in the significance of grain size parameters: Journal of Sedimentary Petrology, v. 27, no. 1, p. 3–26. https://doi.org/10.1306/74D70646-2B21-11D7-8648000102C1865D

Loewen, M.W., Wallace, K.L., Lubbers, Jordan, Ruth, Dawn, Izbekov, P.E., Larsen, J.F., and Graham, Nathan, 2023, Glass electron microprobe analyses methods, precision, and accuracy for tephra studies in Alaska: Alaska Division of Geological & Geophysical Surveys Miscellaneous Publication 174. https://doi.org/10.14509/31045

Mastin, L.G., Van Eaton, A.R., and Schwaiger, H.F., 2020, A probabilistic assessment of tephra-fall hazards at Hanford, Washington, from a future eruption of Mount St. Helens: U.S. Geological Survey Open-File Report 2020–1133, 54 p. https://doi.org/10.3133/ofr20201133

Stratton, J.A., 2015, Electromagnetic theory: Hoboken, New Jersey, John Wiley & Sons, Inc., 615 p.

Schmith, Johanne, and Swanson, D.A., 2023, Complex styles of phreatomagmatic explosions at Kīlauea Volcano, Hawaii, controlled by magma structure: Frontiers in Earth Science, v. 11, 25 p. https://doi.org/10.3389/feart.2023.1153288

Vogel, Andreas, Diplas, Spyros, Durant, A.J., Azar, A.S., Sunding, M.F., Rose, W.I., Sytchkova, Anna, Bonadonna, Costanza, Krüger, Kristin, and Stohl, Andreas, 2017, Reference data set of volcanic ash physicochemical and optical properties: Journal of Geophysical Research Atmospheres, v. 122, no. 17, p. 9,485–9,514. https://doi.org/10.1002/2016JD026328